Journal of Solid Mechanics Vol. 13, No. 1 (2021) pp. 80-94
DOI: 10.22034/jsm.2020.1895052.1557

Vibration Analysis of a Magneto Thermo Electrical Nano Fiber Reinforced with Graphene Oxide Powder Under Refined Beam Model

R. Selvamani [1,*], J. Rexy [1], F. Ebrahimi [2]

[1]*Department of Mathematics, Karunya Institute of Technology and Sciences, Coimbatore-641114, Tamilnadu, India*
[2]*Department of Mechanical Engineering, Imam Khomieni International University, Qazvin, Iran*

Received 9 November 2020; accepted 24 January 2021

ABSTRACT

The present article express the magneto thermo electric deformation of composite nano fiber reinforced by graphene oxide powder (GOP). To reach the governing equation of the problem a higher-order trigonometric refined beam model is utilized according to Hamilton's principle. The effect of a nonuniform magnetic and thermo piezo electric field is applied to the governing equations by combining the field relations with the displacement field equations. Then, obtained equations are solved by using Galerkin's method to consider the influence of different boundary conditions on the vibrational responses of the fiber. The accuracy and efficiency of the presented model is verified by comparing the results with that of published researches. Further, the effects of different variant on the dimensionless frequency of GOP reinforced magneto piezo thermo elastic composite fibers are highlighted through tables and dispersion curves. The weight fraction of GOP and the magneto thermo electro effects have significant influence in the stiffness of the nano composites.

Keywords : Static stability; Piezo electric fibers; Magneto thermo elastic beam; Graphene oxide powder; Refined trigonometric beam theory; NEMS.

1 INTRODUCTION

In recent years, the usage of grapheme oxide powder (GOP) in composite structures as reinforcements in order to achieve the higher efficiency of the structure has been attracting many researchers in recent years. Graphene and its derivatives as reinforcement in polymer matrix possesses extraordinarily potential due to their supreme mechanical properties, improved reinforcing effects, considerable electrical and thermal conductivities and moderate cost Ni et al. [1]. Emam and Eltaher [2] studied the buckling and post buckling of composite beams in hygrothermal environments and they show that hygrothermal parameter has a great effect on both buckling and post buckling

*Corresponding author.
E-mail address: selvamani@karunya.edu (R.Selvamani)

response of composite beams. Arefi and Zenkour [3] studied the wave propagation analysis of a functionally graded magneto-electro-elastic Nano beam rest on Visco-Pasternak foundation, they identified from the curves that by increasing the non-homogeneous index and wave number tend to decrease in wave propagation phase velocities. Using nonlocal theory, Ke and Wang [4] reported the free vibration of size-dependent magneto–electro-elastic Nano beams. In this study, they found that the natural frequency of Nano beams is not sensitive to the temperature rise. Kheibari and Beni [5] investigated the size dependent electro-mechanical vibration of single-walled piezoelectric nanotubes using thin shell model. Selvamani and Ebrahimi [6] analysed the axisymmetric Vibration in a Submerged, Piezoelectric Rod Coated with Thin Film with the aid of Bessel function. Ke et.al [7] reported the thermo-electro-mechanical vibration of size-dependent piezoelectric cylindrical Nano shells under various boundary conditions. From their model, they found that the nonlocal effect and thermoelectric loading have a significant effect on natural frequencies of piezoelectric Nano shells. Ebrahimi et al. [8] reported the thermal buckling analysis of magneto electro elastic porous FG beam in thermal environment. Thermal buckling of magneto-electro-elastic piezoelectric nanobeams was read by Alibeigi et al. [9] and they exposed the truth that the critical buckling temperature of the clamped nanobeam with uniform temperature rise is lower than that with linear temperature variation. Liu et al. [10] reported the three dimensional buckling and free vibration analyses of initially stressed functionally graded graphene reinforced composite cylindrical shell. Shen et al. [11] studied the buckling and post buckling of functionally graded graphene-reinforced composite laminated plates in thermal environments and they concluded with the highlights that the buckling loads as well as the post buckling strength of the GRC laminated plates may be enhanced through piece-wise functionally graded distribution of graphene. Zhang et al. [12] investigated the Mechanical analysis of functionally graded graphene oxide-reinforced composite beams based on the first-order shear deformation theory and they showed that GOP is superior to the single-walled carbon nanotubes and multi-walled carbon nanotubes in reinforcing the mechanical behaviors of polymer nanocomposite. García-Macías et al. [13] reported the Bending and free vibration analysis of functionally graded graphene vs. carbon nanotube reinforced composite plates. In their study, they revealed that functionally graded Graphite Nano Platelets can tune the overall stiffness of the composite plates.

Martin-Gallego et al. [14] introduced the comparison of filler percolation and mechanical properties in graphene and carbon nanotubes filled epoxy nanocomposites. Im and Kim [15] developed the thermal conductivity of a graphene oxide–carbon nanotube hybrid/epoxy composite and they explored that the wetting process utilizing the surface energy of GO and MWCNTs for preparing conductive polymer composites is appropriate for fabricating highly concentrated composites containing a GO/MWCNT hybrid filler with reasonably high mechanical properties. Ebrahimi et al. [16] analyzed the thermal vibration analysis of embedded graphene oxide powder-reinforced nanocomposite plates and they revealed that the frequency responses of the nanocomposite plates in a thermal environment dramatically depend on the distribution pattern of the GOPs. Ebrahimi et al. [17] constructed the modeling vibration behavior of embedded graphene-oxide powder-reinforced nanocomposite plates in thermal environment. In this research, they observed that the damping coefficient had a stiffness-softening effect on the structure in a way that during the inclusion of the damping coefficient the natural frequencies of the plate reduced as far as reached to zero in a critical point. Ebrahimi et al. [18] studied the vibration analysis of magnetically affected graphene oxide-reinforced nanocomposite beams. From their conclusion, they presented that the dimensionless frequency can be amplified using higher weight fraction for GOPs. Mao and Zhang [19] analyzed the linear and nonlinear free and forced vibrations of grapheme reinforced piezoelectric composite plate under external voltage excitation and they illustrated that the great potential of using GPLs in achieving smart structures with significantly improved structural stiffness. Mao and Zhang [20] developed the Buckling and post-buckling analyses of functionally graded graphene reinforced piezoelectric plate subjected to electric potential and axial forces, they found that the GPLs have a significantly enhancing influence on the buckling and post-buckling strength of the FG-GRP plates. Ebrahimi et al. [21] observed the bending analysis of magneto-electro piezoelectric Nano beams system under hygro-thermal loading. Ebrahimi et al. [22] developed the dynamic characteristics of hygro-magneto-thermo-electrical Nano beam with non-ideal boundary conditions. Ebrahimi et al. [23] reported the thermo-electro-elastic nonlinear stability analysis of viscoelastic double-piezo nanoplates under magnetic field. Mahaveer sree jayan and selvamani [24] studied the chirality and small-scale effects on embedded thermo elastic carbon nanotube conveying fluid. Mahaveer sree jayan et al. [25] analysed the nonlocal dispersion analysis of a fluid conveying thermo elastic armchair single walled carbon nanotube under moving harmonic excitation, they shown that the dynamic displacement of fluid conveying SWCNT ratio is significantly affected by the load velocity and the excitation frequency. Rexy et al. [26] investigated the thermo piezoelectric sound waves in a nanofiber using Timoshenko beam theory incorporated with surface effect, they shown that the surface effect gives significant contribution to the physical variables. Selvamani et al. [27] reported the sound wave propagation in a Multiferroic thermo elastic nano fiber under the influence of surface effect and parametric excitation, they found that the frequency grows in the

presence of surface effect and decay as length increases both in Euler's and Timoshenko beam theory. Calin et al. [28] investigated on the improved rigidity of composite circular plates through radial ribs. Vlase et al. [29] analysed the motion equation for a flexible one-dimensional element used in the dynamical analysis of a multibody system. Bhatti et al. [30] studied the swimming of motile gyro tactic microorganisms and nanoparticles in blood flow through anisotropically tapered arteries, they found that the shear stress at the wall is reduced due to an increment in the height of stenosis and the bio convection Rayleigh number.

2 FORMULATION OF THE PROBLEM

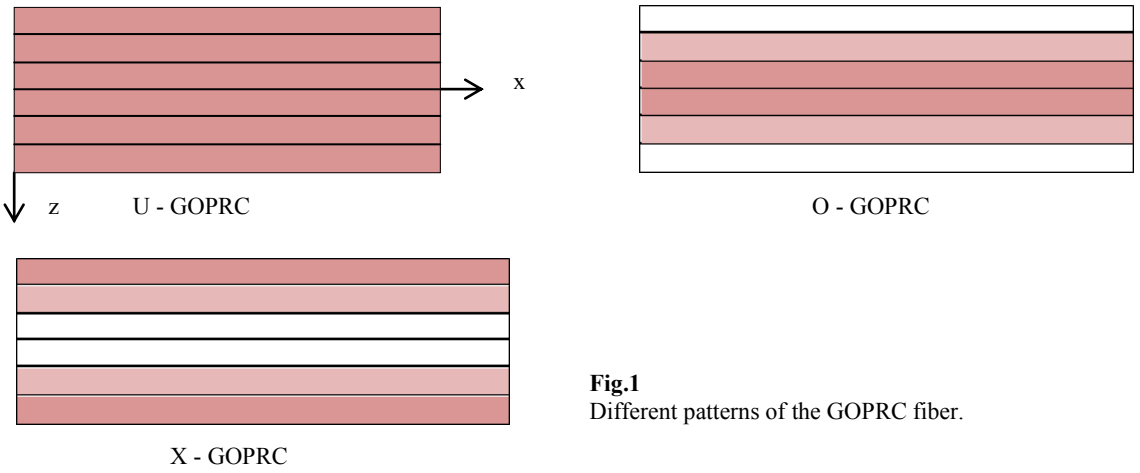

Fig.1
Different patterns of the GOPRC fiber.

In this study, three different patterns of reinforcement distribution are considered as shown in Figure 1.Through different patterns, the reinforcements are introduced in the matrix. These patterns can be generated by putting the fibers in a series of specified positions which can be calculated with (Ebrahimi et al. [18])

$$\begin{aligned} V_{GOP} &= V_{GOP}^{*} && \text{GOPR-U}, \\ V_{GOP} &= \left(2-4\frac{|z|}{h}\right)V_{GOP}^{*} && \text{GOPR-O}, \\ V_{GOP} &= 4\frac{|z|}{h}V_{GOP}^{*} && \text{GOPR-X}, \end{aligned} \tag{1}$$

where the total volume fraction V_{GOP}^{*} is defined as:

$$V_{GOP}^{*} = \frac{W_{GOP}}{W_{GOP} + (\rho_{GOP}/\rho_{M})(1-W_{GOP})} \tag{2}$$

In which the subscript GOP and *M* represents the GOP reinforcements and the matrix, respectively. In addition, ρ stands for mass density and W_{GOP} denotes GOP weight fraction. Now, the Young's modulus can be written as (Zhang et al. [12])

$$E_{eff} = 0.49E_{l} + 0.51E_{t} \tag{3}$$

where E_{l} and E_{t} are longitudinal and transverse Young's modulus of the composite, respectively. They can be calculated as:

$$E_l = \frac{1+\xi_l \eta_l V_{GOP}}{1-\eta_l V_{GOP}} \times E_M \ , \ E_t = \frac{1+\xi_t \eta_t V_{GOP}}{1-\eta_t V_{GOP}} \times E_M \, , \tag{4}$$

$$\eta_l = \frac{\left(E_{GOP}/E_M\right)-1}{\left(E_{GOP}/E_M\right)+\xi_l} \times E_M \ , \ \eta_t = \frac{\left(E_{GOP}/E_M\right)-1}{\left(E_{GOP}/E_M\right)+\xi_t} \times E_M \, , \tag{5}$$

In which E_{GOP} and E_M stand for GOP's and the matrix of Young's modulus, respectively. Also, the explicit form of the geometry factors $\left(\xi_l, \xi_t\right)$ is calculated as:

$$\xi_l = \xi_t = \frac{2d_{GOP}}{h_{GOP}} \tag{6}$$

In which d_{GOP} and h_{GOP} are related to diameter and thickness of GOP's respectively. Now, the effective Poisson's ratio of the composite can be achieved by using the rule of mixture as follows:

$$v_{eff} = v_{GOP} V_{GOP} + v_M V_M \tag{7}$$

In which V_{GOP} and V_M correspond with the volume fractions of GOP's and matrix. From Eq. (7), it is referred that the effective mass density can be computed in the same form as Poisson's ratio. The volume fractions are related to each other as:

$$V_{GOP} + V_M = 1 \tag{8}$$

The coefficient of thermal expansion (CTE) for the GOPR nano composite is reached as:

$$\alpha_{eff} = \alpha_M + \frac{\alpha_M + \alpha_{GOP}}{\frac{1}{K_M} + \frac{1}{K_{GOP}}} \left[\frac{1}{K_{eff}} + \frac{1}{K_M} \right] \tag{9}$$

Here K is the bulk moduli and α is the CTE. Also, the M and GOP subscripts are referred to the matrix and grapheme oxide powder, respectively.

3 REFINED HIGHER-ORDER TRIGONOMETRY BEAM THEORY

Due to the limitation in slenderness ratio , the researchers remodelled a higher-order shear deformable beam theory which are able to estimate the shear stress and strain of the beam. For this purpose, a shape function is presented in each theory. Herein, the refined form of sinusoidal beam theory is utilized to achieve the kinematic relations of the beam. According to this theory, the displacement field of a beam can be written as:

$$u_x(x,z,t) = u(x,t) - z\frac{\partial w_b}{\partial x} - f(z)\frac{\partial w_s}{\partial x} \tag{10}$$

$$u_z(x,z,t) = w_b(x,t) + w_s(x,t) \tag{11}$$

where u is longitudinal displacement and w_b, w_s are bending and shear deflections, respectively. The corresponding shape function of the employed theory can be expressed as:

$$f(z) = z - \frac{h}{\pi}\sin\left(\frac{\pi z}{h}\right) \tag{12}$$

The nonzero strains Π of the beam can be expressed by the following equations (Ebrahimi et al. [18])

$$\Pi_{xx} = \frac{\partial u}{\partial x} - z\,\frac{\partial^2 w_b}{\partial x^2} - f(z)\frac{\partial^2 w_s}{\partial x^2} \tag{13}$$

$$\Pi_{xz} = g(z)\frac{\partial w_s}{\partial x} \tag{14}$$

where $g(z) = 1 - \dfrac{df(z)}{dz}$

For the purpose of satisfying Maxwell's equation in the quasi-static approximation, the applied external electric potential is modelled as a function of combined linear and cosine variations as follows:

$$\phi(x,z,t) = -\cos(\xi z)\phi(x,t) + \frac{2z}{h}v \tag{15}$$

Now, based on Eq. (15), the electric field (E_x, E_z) and (ϕ) electric potential can be related to each other as follows:

$$E_x = -\phi_{,x} = \cos(\xi z)\frac{\partial \phi}{\partial x} \tag{16}$$

$$E_z = -\phi_{,z} = -\xi\sin(\xi z)\phi - \frac{2v}{h} \tag{17}$$

4 HAMILTON'S PRINCIPLE

Now, Hamilton's principle can be defined as:

$$\int_0^t \delta(R - S + T)dt = 0 \tag{18}$$

where *R, S*, and *T* account for strain energy, kinetic energy, and work done by external forces, respectively. The variation of strain energy is written as:

$$\delta U = \int(\Pi_{xx}\,\delta\amalg_{xx} + \Pi_{xz}\,\delta\amalg_{xz} - D_x\delta E_x - D_z\delta E_z)dv \tag{19}$$

where $\prod_{xx}$ is the component of normal stress. D_x, D_z are the electric displacements. Substituting Eqs. (13) – (17) in Eq. (19) yields

$$\delta R = \int_0^L \left(N\frac{\partial \delta u}{\partial x} - M_b\frac{\partial^2 \delta w_b}{\partial x^2} - M_s\frac{\partial^2 \delta w_s}{\partial x^2} + Q\frac{\partial \delta w_s}{\partial x}\right)dx + \int_0^L\int_{-h/2}^{h/2}\left(-D_x\cos(\xi z)\delta\left(\frac{\partial \phi}{\partial x}\right) + D_z\xi\sin(\xi z)\delta\phi\right)dz\,dx\ , \tag{20}$$

In which the stress resultants *N,* M_b , M_s and *Q* are expressed as:

$$\left[N, M_b, M_s\right] = \int_A \left[1, z, f(z)\right] \prod_{xx} dA \tag{21}$$

$$Q = \int_A g(z) \prod_{xz} dA \tag{22}$$

Moreover, the variation of the kinetic energy can be formulated as (Ebrahimi et al. [18])

$$\delta S = \int_V \left(\dot{u}_x \, \delta \dot{u}_x + \dot{u}_z \, \delta \dot{u}_z \right) \rho(z) dV \tag{23}$$

$$= \int_0^L \left(\begin{array}{l} I_0 \left(\frac{\partial u}{\partial t} \frac{\partial \delta u}{\partial t} + \frac{\partial \left(w_b + w_s\right)}{\partial t} \frac{\partial \delta \left(w_b + w_s\right)}{\partial t} \right) - I_1 \left(\frac{\partial u}{\partial t} \frac{\partial^2 \delta w_b}{\partial x \, \partial t} + \frac{\partial^2 w_b}{\partial x \, \partial t} \frac{\partial \delta u}{\partial t} \right) \\ -J_1 \left(\frac{\partial u}{\partial t} \frac{\partial^2 \delta w_s}{\partial x \, \partial t} + \frac{\partial^2 w_s}{\partial x \, \partial t} \frac{\partial \delta u}{\partial t} \right) + I_2 \left(\frac{\partial^2 w_b}{\partial x \, \partial t} \frac{\partial^2 \delta w_b}{\partial x \, \partial t} \right) + K_2 \left(\frac{\partial^2 w_s}{\partial x \, \partial t} \frac{\partial^2 \delta w_s}{\partial x \, \partial t} \right) \\ +J_2 \left(\frac{\partial^2 w_b}{\partial x \, \partial t} \frac{\partial^2 \delta w_s}{\partial x \, \partial t} + \frac{\partial^2 w_s}{\partial x \, \partial t} \frac{\partial^2 \delta w_b}{\partial x \, \partial t} \right) \end{array} \right) dx \ , \tag{24}$$

where the mass moments of inertia used in Eq. (24) can be calculated as:

$$\left[I_0, I_1, J_1, I_2, J_2, K_2\right] = \int_A \left[1, z, f(z), z^2, z f(z), f^2(z)\right] \rho_{eff} dA \ , \tag{25}$$

Besides, in this research, the nanocomposite is assumed to be subjected to an in-plane magnetic field. Thus, the Maxwell's magnetic induction rules are extended to achieve the equivalent body force applied to the beam. Herein, the longitudinal magnetic field is considered to be

$$H = \left(H_x, 0, 0\right) \ , \ H = \left(H_x, 0, 0\right), \ H_x = \overline{H_x} \sin\left(\frac{\pi x}{L} \right) \tag{26}$$

where $\overline{H_x}$ is the amplitude of the longitudinal magnetic field; Maxwell's relation can be developed as:

$$f_z = \eta \left[\nabla \times \left(\nabla \times \left(\vec{u} \times \vec{H} \right) \right) \right] \vec{H} \tag{27}$$

$$= \eta \left[H_x^2 \frac{\partial^2 \left(w_b + w_s\right)}{\partial x^2} + 2 H_x \frac{\partial H_x}{\partial x} \frac{\partial \left(w_b + w_s\right)}{\partial x} + H_x \frac{\partial^2 H_x}{\partial x^2} \left(w_b + w_s\right) \right] \tag{28}$$

where $\vec{u} = \left(u_x, 0, u_z\right)$ is displacement vector and η is magnetic permeability. By inserting the displacement field in the above equation, the resultant Lorentz force can be achieved as:

$$f_{Lz} = \int_A f_z dA = \psi_1 \frac{\partial^2 \left(w_b + w_s\right)}{\partial x^2} + \psi_2 \frac{\partial \left(w_b + w_s\right)}{\partial x} - \psi_3 \left(w_b + w_s\right) \tag{29}$$

where

$$\psi_1 = \eta A \overline{H_x}^2 \sin^2\left(\frac{\pi x}{L}\right),$$
$$\psi_2 = 2\eta A \left(\frac{\pi}{L}\right)\overline{H_x}^2 \sin\left(\frac{\pi x}{L}\right)\cos\left(\frac{\pi x}{L}\right),$$
$$\psi_3 = \eta A \left(\frac{\pi}{L}\right)^2 \overline{H_x}^2 \sin^2\left(\frac{\pi x}{L}\right),$$

Now, the variation of work done by external forces can be formulated a

$$\delta T = \int_0^L \begin{pmatrix} N^T \dfrac{\partial\left(w_b + w_s\right)}{\partial x}\dfrac{\partial\delta\left(w_b + w_s\right)}{\partial x} + \psi_1 \dfrac{\partial\left(w_b + w_s\right)}{\partial x}\dfrac{\partial\delta\left(w_b + w_s\right)}{\partial x} + \psi_2\left(w_b + w_s\right)\dfrac{\partial\delta\left(w_b + w_s\right)}{\partial x} \\ -\psi_3\left(w_b + w_s\right)\delta\left(w_b + w_s\right) \end{pmatrix} dx \tag{30}$$

The thermal loading (N^T) can be defined as:

$$N^T = \int_{\frac{-h}{2}}^{\frac{h}{2}} \left(\frac{E_{eff}}{1-\nu_{eff}}\alpha_{eff}\,\Delta T\right) dz \tag{31}$$

Therefore, once substituting Eqs. (20), (24), and (30) in Eq. (18) and solving for the nontrivial response, the Euler–Lagrange equations of this problem are reached as:

$$\frac{\partial N}{\partial x} = I_0 \frac{\partial^2 u}{\partial t^2} - I_1 \frac{\partial^3 w_b}{\partial x\,\partial t^2} - J_1 \frac{\partial^3 w_s}{\partial x\,\partial t^2}\ , \tag{32}$$

$$\begin{aligned} &\frac{\partial^2 M_b}{\partial x^2} - N^T \frac{\partial^2\left(w_b + w_s\right)}{\partial x^2} - \psi_1 \frac{\partial^2\left(w_b + w_s\right)}{\partial x^2} - \psi_2 \frac{\partial\left(w_b + w_s\right)}{\partial x} + \psi_3\left(w_b + w_s\right) \\ &= -I_0 \frac{\partial^2\left(w_b + w_s\right)}{\partial t^2} + I_1 \frac{\partial^3 u}{\partial x\,\partial t^2} - I_2 \frac{\partial^4 w_b}{\partial x^2 \partial t^2} - J_2 \frac{\partial^4 w_s}{\partial x^2 \partial t^2}\ , \end{aligned} \tag{33}$$

$$\begin{aligned} &\frac{\partial^2 M_s}{\partial x^2} - \frac{\partial Q}{\partial x} - N^T \frac{\partial^2\left(w_b + w_s\right)}{\partial x^2} - \psi_1 \frac{\partial^2\left(w_b + w_s\right)}{\partial x^2} - \psi_2 \frac{\partial\left(w_b + w_s\right)}{\partial x} + \psi_3\left(w_b + w_s\right) \\ &= -I_0 \frac{\partial^2\left(w_b + w_s\right)}{\partial t^2} + J_1 \frac{\partial^3 u}{\partial x\,\partial t^2} - K_2 \frac{\partial^4 w_s}{\partial x^2 \partial t^2} - J_2 \frac{\partial^4 w_b}{\partial x^2 \partial t^2}\ , \end{aligned} \tag{34}$$

$$\int_{-h/2}^{h/2} \left(-\cos\left(\xi z\right)\frac{\partial D_x}{\partial x} + D_z\,\xi \sin\left(\xi z\right)\right) dz = 0\ , \tag{35}$$

5 CONTROLLING EQUATIONS

In this sub-section, the stress–strain relations of isotropic materials are reviewed for the purpose of deriving the fundamental elastic equations of solids. Here, the following constitutive equations can be expressed

$$\prod_{ij} = c_{ijkl} \coprod_{kl} - e_{ijk} E_k\ ,\ c_{ijkl} \tag{36}$$

Corresponds with the components of the fourth order elasticity tensor. Whenever extending the aforementioned equation for a shear deformable beam, the following relations can be reached

$$\prod_{xx} = E_{eff} \coprod_{xx} - e_{31} E_z \ , \tag{37}$$

$$\prod_{xz} = G_{eff} \coprod_{xz} - e_{15} E_x \ , \tag{38}$$

$$D_x = e_{15} \coprod_{xz} + s_{11} E_x \ , \tag{39}$$

$$D_z = e_{31} \coprod_{xx} + s_{33} E_z \ , \tag{40}$$

In which E_{eff} and G_{eff} denote the Young's and shear moduli of the nanocomposite, respectively. Integrating from Eqs. (37)-(40) over the cross-section area of the beam, the following equations

$$N = A \frac{\partial u}{\partial x} - B \frac{\partial^2 w_b}{\partial x^2} - B_s \frac{\partial^2 w_s}{\partial x^2} - A_{31} \phi - A_{33} A \ , \tag{41}$$

$$M_b = B \frac{\partial u}{\partial x} - D \frac{\partial^2 w_b}{\partial x^2} - D_s \frac{\partial^2 w_s}{\partial x^2} - B_{31} \phi \ , \tag{42}$$

$$M_s = B_s \frac{\partial u}{\partial x} - D_s \frac{\partial^2 w_b}{\partial x^2} - H_s \frac{\partial^2 w_s}{\partial x^2} - E_{31} \phi \ , \tag{43}$$

$$Q = A_s \frac{\partial w_s}{\partial x} - A_E \frac{\partial \phi}{\partial x} \ , \tag{44}$$

$$\int_A D_x \cos(\xi z) dA = A_{15} \frac{\partial w_s}{\partial x} + F_{11} \frac{\partial \phi}{\partial x} \ , \tag{45}$$

$$\int_A D_z \xi \sin(\xi z) dA = A_{31} \frac{\partial u}{\partial x} - B_{31} \frac{\partial^2 w_b}{\partial x^2} - E_{31} \frac{\partial^2 w_s}{\partial x^2} - F_{22} - F_{33} \phi \ , \tag{46}$$

where

$$[A, B, D, B_s, D_s H_s] = \int_A \left[1, z, z^2, f(z), zf(z), f^2(z)\right] E_{eff} dA \ ,$$

$$A_s = \int_A g^2(z) G_{eff} dA \ ,$$

$$A_E = \int_A e_{15} g(z) \cos(\xi z) dz \ ,$$

$$[A_{31}, B_{31}, E_{31}] = \int_A e_{31} [1, z, f(z)] \xi \sin(\xi z) dA \ ,$$

$$[F_{11}, F_{22}, F_{33}] = \int_A \left[s_{11} \cos^2(\xi z), s_{33} \xi \sin(\xi z), s_{33} \xi^2 \sin^2(\xi z)\right] dA \ ,$$

$$A_{33} = \int_A e_{31} \frac{2v}{h} dA \ ,$$

Now, by inserting Eqs. (41)–(46) in Eqs. (32)–(35), the governing equations of GOPRC beams can be expressed in the following form

$$A\frac{\partial^2 u}{\partial x^2}-B\frac{\partial^3 w_b}{\partial x^3}-B_s\frac{\partial^3 w_s}{\partial x^3}-A_{31}\frac{\partial \phi}{\partial x}+I_0\frac{\partial^2 u}{\partial t^2}-I_1\frac{\partial^3 w_b}{\partial x\,\partial t^2}-J_1\frac{\partial^3 w_s}{\partial x\,\partial t^2}=0 \tag{47}$$

$$\begin{aligned}&B\frac{\partial^3 u}{\partial x^3}-D\frac{\partial^4 w_b}{\partial x^4}-D_s\frac{\partial^4 w_s}{\partial x^4}-B_{31}\frac{\partial^2 \phi}{\partial x^2}-N^T\frac{\partial^2\left(w_b+w_s\right)}{\partial x^2}-\psi_1\frac{\partial^2\left(w_b+w_s\right)}{\partial x^2}-\psi_2\frac{\partial\left(w_b+w_s\right)}{\partial x}+\psi_3\left(w_b+w_s\right)\\&+I_0\frac{\partial^2\left(w_b+w_s\right)}{\partial t^2}-I_1\frac{\partial^3 u}{\partial x\,\partial t^2}+I_2\frac{\partial^4 w_b}{\partial x^2\partial t^2}+J_2\frac{\partial^4 w_s}{\partial x^2\partial t^2}=0\ ,\end{aligned} \tag{48}$$

$$\begin{aligned}&B_s\frac{\partial^3 u}{\partial x^3}-D_s\frac{\partial^4 w_b}{\partial x^4}-H_s\frac{\partial^4 w_s}{\partial x^4}-A_s\frac{\partial^2 w_s}{\partial x^2}-E_{31}\frac{\partial^2 \phi}{\partial x^2}-A_E\frac{\partial^2 \phi}{\partial x^2}-N^T\frac{\partial^2\left(w_b+w_s\right)}{\partial x^2}-\psi_1\frac{\partial^2\left(w_b+w_s\right)}{\partial x^2}\\&-\psi_2\frac{\partial\left(w_b+w_s\right)}{\partial x}+\psi_3\left(w_b+w_s\right)-I_0\frac{\partial^2\left(w_b+w_s\right)}{\partial t^2}-J_1\frac{\partial^3 u}{\partial x\,\partial t^2}+K_2\frac{\partial^4 w_s}{\partial x^2\partial t^2}+J_2\frac{\partial^4 w_b}{\partial x^2\partial t^2}=0\ ,\end{aligned} \tag{49}$$

$$A_{15}\frac{\partial^2 w_s}{\partial x^2}+F_{11}\frac{\partial^2 \phi}{\partial x^2}-A_{31}\frac{\partial u}{\partial x}+B_{31}\frac{\partial^2 w_b}{\partial x^2}+E_{31}\frac{\partial^2 w_s}{\partial x^2}+F_{33}=0 \tag{50}$$

6 SOLUTION OF THE PROBLEM

Here, on the basis the Navier method, an analytical solution of the governing equations for free vibration of a simply supported magneto–electro–thermo-elastic FG Nanofiber is presented. To satisfy governing equations of motion, the displacement variables are adopted to be of the form

$$u(x,t)=\sum_{n=1}^{\infty}U_n\cos\left(\frac{n\pi}{L}x\right)e^{i\omega_n t}\ , \tag{51}$$

$$w_b(x,t)=\sum_{n=1}^{\infty}W_{bn}\sin\left(\frac{n\pi}{L}x\right)e^{i\omega_n t}\ , \tag{52}$$

$$w_s(x,t)=\sum_{n=1}^{\infty}W_{sn}\sin\left(\frac{n\pi}{L}x\right)e^{i\omega_n t}\ , \tag{53}$$

$$\phi(x,t)=\sum_{n=1}^{\infty}\phi_n\sin\left(\frac{n\pi}{L}x\right)e^{i\omega_n t}\ , \tag{54}$$

where U_n, W_{bn}, W_{sn} and ϕ_n are the unknown Fourier coefficients to be determined for each n value. Using Eqs. (47)-(50) the analytical solution can be obtained from the following equations:

$$[V]-\omega_n^2[W]=0\ , \tag{55}$$

where

$$v_{11}=-A\left(\frac{n\pi}{L}\right)^2\ ,\quad v_{12}=B\left(\frac{n\pi}{L}\right)^3\ ,\quad v_{13}=B_s\left(\frac{n\pi}{L}\right)^3\ ,\quad v_{14}=-A_{31}\left(\frac{n\pi}{L}\right)\ ,\quad v_{21}=B\left(\frac{n\pi}{L}\right)^3\ ,$$
$$v_{22}=-D\left(\frac{n\pi}{L}\right)^4+N^T\left(\frac{n\pi}{L}\right)^2+\psi_1\left(\frac{n\pi}{L}\right)^2-2\eta A\left(\frac{\pi}{L}\right)\overline{H_x}^2\cos^2\left(\frac{n\pi}{L}x\right)+\psi_3\ ,$$

$$v_{23}=-D_s\left(\frac{n\pi}{L}\right)^4+N^T\left(\frac{n\pi}{L}\right)^2+\psi_1\left(\frac{n\pi}{L}\right)^2-2\eta A\left(\frac{\pi}{L}\right)\overline{H_x}^2\cos^2\left(\frac{n\pi}{L}x\right)+\psi_3\ ,$$

$$v_{24}=B_{31}\left(\frac{n\pi}{L}\right)^2\ ,\quad v_{31}=B_s\left(\frac{n\pi}{L}\right)^3\ ,$$

$$v_{32}=-D_s\left(\frac{n\pi}{L}\right)^4+N^T\left(\frac{n\pi}{L}\right)^2+\psi_1\left(\frac{n\pi}{L}\right)^2-2\eta A\left(\frac{\pi}{L}\right)\overline{H_x}^2\cos^2\left(\frac{n\pi}{L}x\right)+\psi_3\ ,$$

$$v_{33}=-H_s\left(\frac{n\pi}{L}\right)^4+A_s\left(\frac{n\pi}{L}\right)^2+N^T\left(\frac{n\pi}{L}\right)^2+\psi_1\left(\frac{n\pi}{L}\right)^2-2\eta A\left(\frac{\pi}{L}\right)\overline{H_x}^2\cos^2\left(\frac{n\pi}{L}x\right)+\psi_3\ ,$$

$$v_{34}=\left(E_{31}+A_E\right)\left(\frac{n\pi}{L}\right)^2\ ,\quad v_{41}=A_{31}\left(\frac{n\pi}{L}\right)\ ,\quad v_{42}=-B_{31}\left(\frac{n\pi}{L}\right)^2\ ,\quad v_{43}=-\left(A_{15}+E_{31}\right)\left(\frac{n\pi}{L}\right)^2\ ,$$

$$v_{44}=-F_{11}\left(\frac{n\pi}{L}\right)^2+F_{33}\ ,$$

$$w_{11}=-I_0\ ,\quad w_{12}=I_1\left(\frac{n\pi}{L}\right)\ ,\quad w_{13}=J_1\left(\frac{n\pi}{L}\right)\ ,\ w_{14}=0\ ,\ w_{21}=-I_1\left(\frac{n\pi}{L}\right)\ ,$$

$$w_{22}=-I_0\omega_n^2+I_2\left(\frac{n\pi}{L}\right)^2\ ,\ w_{23}=-I_0\omega_n^2+J_2\left(\frac{n\pi}{L}\right)^2\ ,\ w_{24}=0\ ,\ w_{31}=-J_1\left(\frac{n\pi}{L}\right)\ ,$$

$$w_{32}=I_0\omega_n^2+J_2\left(\frac{n\pi}{L}\right)^2\ ,\ w_{33}=I_0\omega_n^2+K_2\left(\frac{n\pi}{L}\right)^2\ ,\ w_{41}=0,\ w_{42}=0,\ w_{43}=0,\ w_{44}=0\ .$$

7 NUMERICAL DISCUSSION

In this section, some dispersion curves and tables are presented to clarify the effect of various parameters on the vibration responses of GOPRC fibers. Basically, the fiber is supposed to be made of epoxy and it is reinforced with GOP fibers. The material properties of the constituent materials are chosen as the same as those presented by Zhang et al [12]. Also, the fiber's thickness is taken as $h=5cm$ Moreover, magnetic permeability is considered to be $\eta=4\pi\times10^{-7}$. Furthermore, the results of comparison of the present results with those of former researches reveal that this model is accurate enough to estimate the natural frequency of nanocomposite fibers.

Table 1 indicates comparison of dimensionless frequency of S-S graphene oxide powder reinforced composite (GOPRC) beams with $W_{GOP}=0.3\%$ with the published works (Zhang et al. [12] and Ebrahimi et al. [18]) and reliable agreement can be observed. In Table 2 the first ten dimensionless frequencies of graphene oxide powder reinforced composite fibers for different distribution patterns of the graphene oxide powder and various magnetic field intensity with S-S edge condition is obtained.As observed, the influence of changing magnetic field intensity is clearly noticed from the table values and the frequency can be raised by applying high intensity of magnetic field strength. The first ten dimensionless frequencies of graphene oxide powder reinforced composite (GOPRC) fiber for different distributions of the graphene oxide powder and various critical temperature with S-S edge condition is shown in Table 3. Here we can understatnd the fact that the fiber can losses the magnitutde of dimensionless frequency for higher crtical temperature. In addition, one more fact got out from these values is that the system can get larger dynamical response whenever the GOP is placed in pattern X and lesser in other selections.

Figs. 2-4 present the effect of wave number on dimensionless frequency through various GOP weight fractions for different patterns of GOP. From these figures it is evident that the increase in wave number raises the dimensionless frequency via various GOP weight fractions. In addition, it indicates that the higher dynamics in Pattern X followed by O and U. In Figs. 5-7 indicates effects wave number along with GOP weight fraction against dimensionless frequency for different patterns. It can be seen that the dimensionless frequency increases as the value of GOP weight fraction and wave number grows. In addition, the maximum dimensionless frequency is achieved once again in pattern X. Fig. 8 highlight the variation of dimensionless frequency over piezoelectric strain. Based on the wave pattern, it can be seen that dimensionless frequency grows as piezoelectric strain raises through different modes. Fig. 9 highlights the variation of dimensionless frequency over piezoelectric strain through different GOP

weight fraction. From Fig. 9, it is clear that the variation of piezoelectric strain results the raise in dimensionless frequency while the mass of weight fraction is getting low.

Table 1
Comparison of the first dimensionless frequency of S-S graphene oxide powder reinforced composite (GOPRC) beams ($W_{GOP} = 0.3\%$).

L/h		Distribution type		
		X-GOPRC	O-GOPRC	U-GOPRC
10	Zhang et al.[12]	0.3379	0.2921	0.3159
	Ebrahimi et al.[18]	0.3576	0.3013	0.3095
	Present model	0.3518	0.3110	0.3084
15	Zhang et al. [12]	0.2271	0.1959	0.2121
	Ebrahimi et al [18]	0.2411	0.2009	0.2079
	Present model	0.2346	0.2073	0.2290
20	Zhang et al.[12]	0.1708	0.1473	0.1595
	Ebrahimi et al.[18]	0.1815	0.1461	0.1564
	Present model	0.1759	0.1555	0.1642

Table 2
First ten dimensionless frequencies of graphene oxide powder reinforced composite (GOPRC) fibers for different distributions of the graphene oxide powder and various magnetic field intensity constants with S-S edge condition $L/h = 25,\ \Delta T = 10K$, ($W_{GOP} = 1\%$).

	$H_0 = 0.2$			$H_0 = 0.5$		
n	GOPR-U	GOPR-O	GOPR-X	GOPR-U	GOPR-O	GOPR-X
1	0.0214	0.0173	0.0251	0.0222	0.0175	0.0266
2	0.0368	0.0277	0.0441	0.037	0.0278	0.0444
3	0.0524	0.0381	0.0631	0.0525	0.0381	0.0638
4	0.0683	0.0485	0.0835	0.0683	0.0485	0.0836
5	0.0842	0.0590	0.1035	0.0842	0.0590	0.1035
6	0.1002	0.0696	0.1235	0.1002	0.0696	0.1235
7	0.1163	0.0803	0.1435	0.1163	0.0803	0.1436
8	0.1324	0.0910	0.1636	0.1324	0.0910	0.1636
9	0.1485	0.1018	0.1837	0.1485	0.1018	0.1838
10	0.1647	0.1126	0.2039	0.1647	0.1126	0.2039

Table 3
First ten dimensionless frequencies of graphene oxide powder reinforced composite (GOPRC) fiber for different distributions of the graphene oxide powder and various critical temperature with S-S edge condition $L/h = 25,\ H_0 = 0.4,\ (W_{GOP} = 1\%)$.

	$\Delta T = 10K$			$\Delta T = 30K$		
n	GOPR-U	GOPR-O	GOPR-X	GOPR-U	GOPR-O	GOPR-X
1	0.8035	0.4361	1.3951	0.6958	0.3772	1.2104
2	1.7478	0.9497	3.0324	1.6993	0.9232	2.9490
3	2.6758	1.4542	4.6418	2.6439	1.4369	4.5870
4	3.5999	1.9566	6.2446	3.5792	1.9436	6.2038
5	4.5225	2.4581	7.8448	4.5035	2.4478	7.8122
6	5.4443	2.9592	9.4437	5.4286	2.9506	9.4166
7	6.3657	3.4600	11.0419	6.3522	3.4527	11.0187
8	7.2869	3.9607	12.6396	7.2750	3.9543	12.6193
9	8.2078	4.4613	14.2370	8.1973	4.4556	14.2190
10	9.1286	4.9619	15.8342	9.1192	4.9567	15.8180

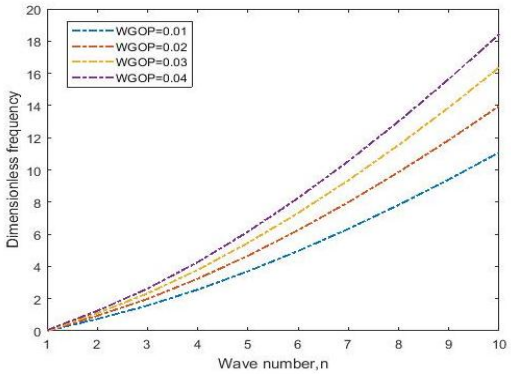

Fig.2
Effects of fiber wave number on dimensionless frequency for GOPR-U fiber.

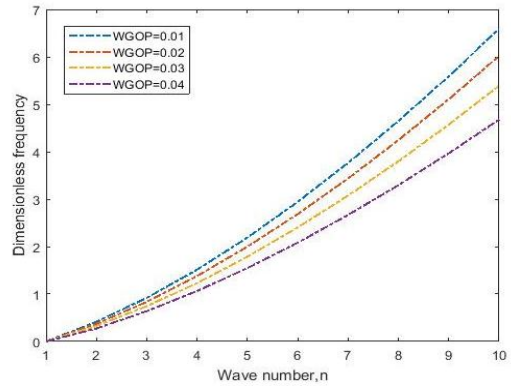

Fig.3
Effects of fiber wave number on dimensionless frequency for GOPR-O fiber.

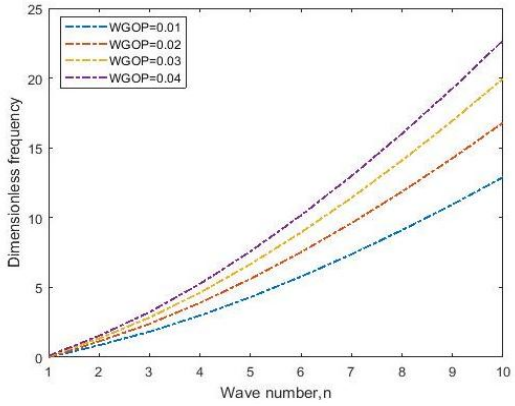

Fig.4
Effects of fiber wave number on dimensionless frequency for GOPR-X fiber.

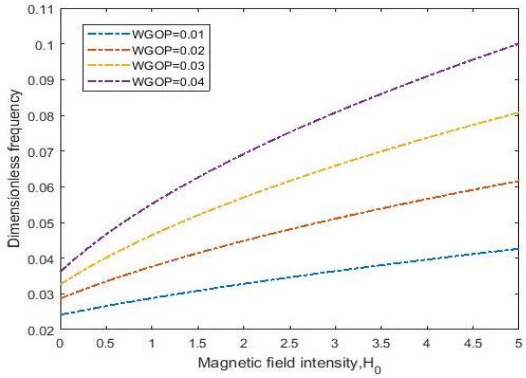

Fig.5
Effects of magnetic field intensity on dimensionless frequency for GOPR-U fiber.

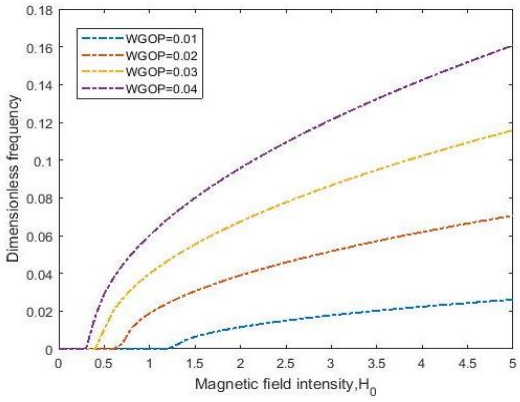

Fig.6
Effects of magnetic field intensity on dimensionless frequency for GOPR-O fiber.

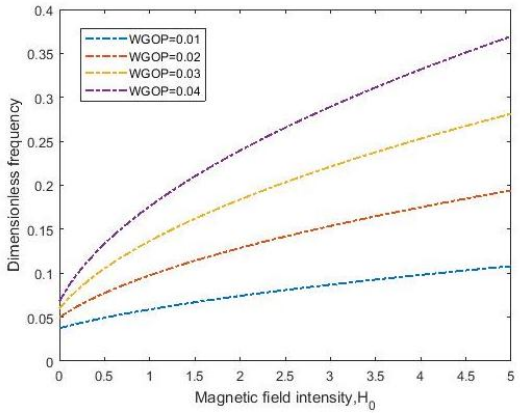

Fig.7
Effects of magnetic field intensity on dimensionless frequency for GOPR-X fiber.

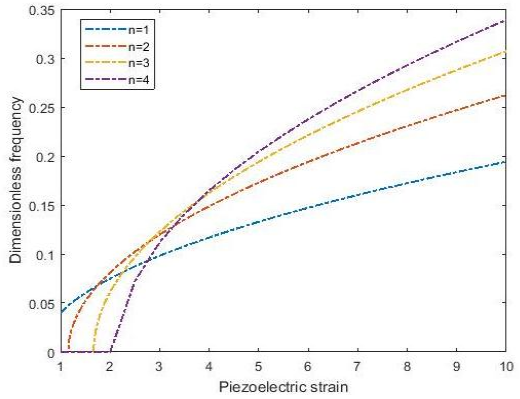

Fig.8
Effects of piezoelectric strain on dimensionless frequency GOPRC fiber via different modes.

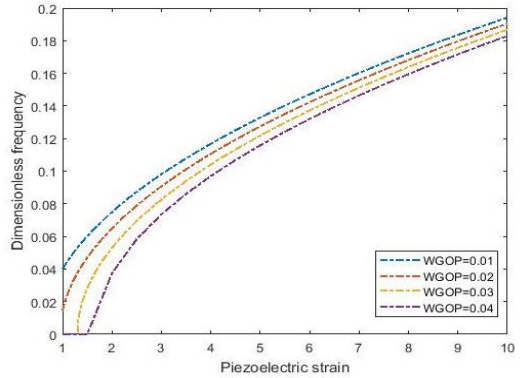

Fig.9
Effects of piezoelectric strain on dimensionless frequency GOPRC fiber via different GOP weight fraction.

8 CONCLUSIONS

The magneto thermo electric deformation of composite nano fiber reinforced by graphene oxide powder (GOP) was investigated in this study. The controlling equation of the problem can be arrived via a higher-order trigonometric refined beam model. The effect of a nonuniform magnetic and thermo piezo electric field is applied to the governing equations by combining the field relations with the displacement field equations. Then, obtained equations are solved by using Galerkin's method to consider the influence of different boundary conditions on the vibrational responses of the fiber.Some of the bolded highlights of this research is as follows.

- The dimensionless frequency can be amplified using higher weight fraction for GOPs.
- The maximum dynamic response can be arrived by choosing GOPRC-X pattern in the presence of magnetic and thermal field.
- The system's dimensionless frequency can be gradually amplified when the magnetic field intensity is increased.
- An increase in the amount of piezoelectric strain results the reduction of GOP weight fraction.
- The dimensionless frequency can be weaken by bigger values of critical temperature.

REFERENCES

[1] Ni Z., Bu H., Zou M., Yi H., Bi K., Chen Y., 2010, Anisotropic mechanical properties of graphene sheets from molecular dynamics, *Physica B: Condensed Matter* **405**: 1301-1306.

[2] Emam S., Eltaher M., 2016, Buckling and postbuckling of composite beams in hygrothermal environments, *Composite Structures* **152**: 665-675.

[3] Arefi M., Zenkour A.M., 2017, Wave propagation analysis of a functionally graded magneto-electro-elastic nanobeam rest on Visco-Pasternak foundation, *Mechanics Research Communications* **79**: 51-62.

[4] Ke L.L., Wang Y.S., 2014, Free vibration of size-dependent magneto–electro-elastic nanobeams based on the nonlocal theory, *Physica E* **63**: 52-61.

[5] Kheibari F., Beni Y.T., 2017, Size dependent electro-mechanical vibration of single-walled piezoelectric nanotubes using thin shell model, *Materials and Design* **114**: 572-583.

[6] Selvamani R., Ebrahimi F., 2020, Axisymmetric vibration in a submerged, piezoelectric rod coated with thin film, *Trends in Mathematics* **2020**: 203-211.

[7] Ke L., Wang Y., Reddy J., 2014, Thermo-electro-mechanical vibration of size-dependent piezoelectric cylindrical nanoshells under various boundary conditions, *Composite Structures* **116**: 626-636.

[8] Ebrahimi F., Jafari A., Selvamani R., 2020, Thermal buckling analysis of magneto electro elastic porous FG beam in thermal environment, *Advanes in Nano Research* **8**(1): 83-94.

[9] Alibeigi B., Beni Y.T., Mehralian F., 2018, On the thermal buckling of magneto-electro-elastic piezoelectric nanobeams, *The European Physical Journal Plus* **133**(3): 133.

[10] Liu D., Kitipornchai S., Chen W., 2018, Three dimensional buckling and free vibration analyses of initially stressed functionally graded graphene reinforced composite cylindrical shell, *Composite Structures* **189**: 560-569.

[11] Shen H.S., Xiang Y., Lin F., 2017, Buckling and postbuckling of functionally graded graphene-reinforced composite laminated plates in thermal environments, *Composites Part B: Engineering* **119**: 67-78.

[12] Zhang Z., Li Y., Wu H., Zhang H., Wu H., Jiang S., Chai G., 2018, Mechanical analysis of functionally graded graphene oxide-reinforced composite beams based on the first-order shear deformation theory, *Mechanics of Advanced Materials and Structures* **27**: 3-11.

[13] Garcia-Macias E., Rodriguez-Tembleque L., Saez A., 2018, Bending and free vibration analysis of functionally graded graphene vs. carbon nanotube reinforced composite plates, *Composite Structures* **186**: 123-138.

[14] Martin-Gallego M., Bernal M.M., Hernandez M., Verdejo R., Lopez-Manchado M.A., 2013, Comparison of filler percolation and mechanical properties in graphene and carbon nanotubes filled epoxy nanocomposites, *European Polymer Journal* **49**: 1347-1353.

[15] Im H., Kim J., 2012, Thermal conductivity of a graphene oxide–carbon nanotube hybrid/epoxy composite, *Carbon* **50**: 5429-5440.

[16] Ebrahimi F., Nouraei M., Dabbagh A., 2020, Thermal vibration analysis of embedded graphene oxide powder-reinforced nanocomposite plates, *Engineering with Computers* **36**: 879-895.

[17] Ebrahimi F., Nouraei M., Dabbagh A., 2019, Modeling vibration behavior of embedded graphene-oxide powder-reinforced nanocomposite plates in thermal environment, *Mechanics Based Design of Structures and Machines* **48**: 1-24.

[18] Ebrahimi F., Dabbagh A., Civalek O., 2019, Vibration analysis of magnetically affected graphene oxide-reinforced nanocomposite beams, *Journal of Vibration and Control* **25**: 2837-2849.

[19] Mao J.J., Zhang W., 2018, Linear and nonlinear free and forced vibrations of grapheme reinforced piezoelectric composite plate under external voltage excitation, *Composite Structures* **203**: 551-565.

[20] Mao J.J., Zhang W., 2019, Buckling and post-buckling analyses of functionally graded graphene reinforced piezoelectric plate subjected to electric potential and axial forces, *Composite Structures* **216**: 392-405.

[21] Ebrahimi F., Karimiasl M., Selvamani R., 2020, Bending analysis of magneto-electro piezoelectric nanobeams system under hygro-thermal loading, *Advances in Nano Research* **8**(3): 203-214.

[22] Ebrahimi F., Kokaba M., Shaghaghi G., Selvamani R., 2020, Dynamic characteristics of hygro-magneto-thermo-electrical nanobeam with non-ideal boundary conditions, *Advances in Nano Research* **8**(2): 169-182.

[23] Ebrahimi F.S., Hosseini H., Selvamani R., 2020, Thermo-electro-elastic nonlinear stability analysis of viscoelastic double-piezo nanoplates under magnetic field, *Structural Engineering and Mechanics* **73**(5): 565-584.

[24] Mahaveer sree jayan M., Selvamani R., 2020, Chirality and small scale effects on embedded thermo elastic carbon nanotube conveying fluid, *Journal of Physics Conference Series* **1597**: 012011.

[25] Mahaveer sree jayan M., Kumar R., Selvamani R., Rexy J., 2020, Nonlocal dispersion analyisis of a fluid conveying thermo elastic armchair single walled carbon nanotube under moving harmonic excitation, *Journal of Solid Mechanics* **12**(1): 189-203.

[26] Rexy J., Selvamani R., Anitha L., 2020, Thermo piezoelectric sound waves in a nanofiber using Timoshenko beam theory incorporated with surface effect, *Journal of Physics: Conference Series* **1597**: 012012.

[27] Selvamani R., Rexy J., Kumar R., 2020, Sound Wave Propagation in a multiferroic thermo elastic Nano Fiber under the influence of surface effect and parametric excitation, *Journal of Solid Mechanics* **12**(2): 493-504.

[28] Calin I., Ochsner A., Vlase S., Marin M., 2019, Improved rigidity of composite circular plates through radial ribs, *Proceedings of the Institution of Mechanical Engineers Part L - Journal of Materials-Design and Applications* **233**(8): 1585-1593.

[29] Vlase S., Marin M., Ochsner A., Scutaru M.L., 2019, Motion equation for a flexible one-dimensional element used in the dynamical analysis of a multibody system, *Continuum Mechanics and Thermodynamics* **31**(3): 715-724.

[30] Bhatti M., Marin M., Zeeshan A., Ellahi R., Sara A., 2020, Swimming of motile gyrotactic microorganisms and nanoparticles in blood flow through anisotropically tapered arteries, *Frontiers in Physics* **8**: 1-12.